ChemSusChem

Supporting Information

Simultaneous Anodic and Cathodic Formate Production in a Paired Electrolyzer by CO_2 Reduction and Glycerol Oxidation

João R. C. Junqueira, Debanjan Das, Ann Cathrin Brix, Stefan Dieckhöfer, Jonas Weidner, Xin Wang, Jialin Shi, and Wolfgang Schuhmann*

XPS results

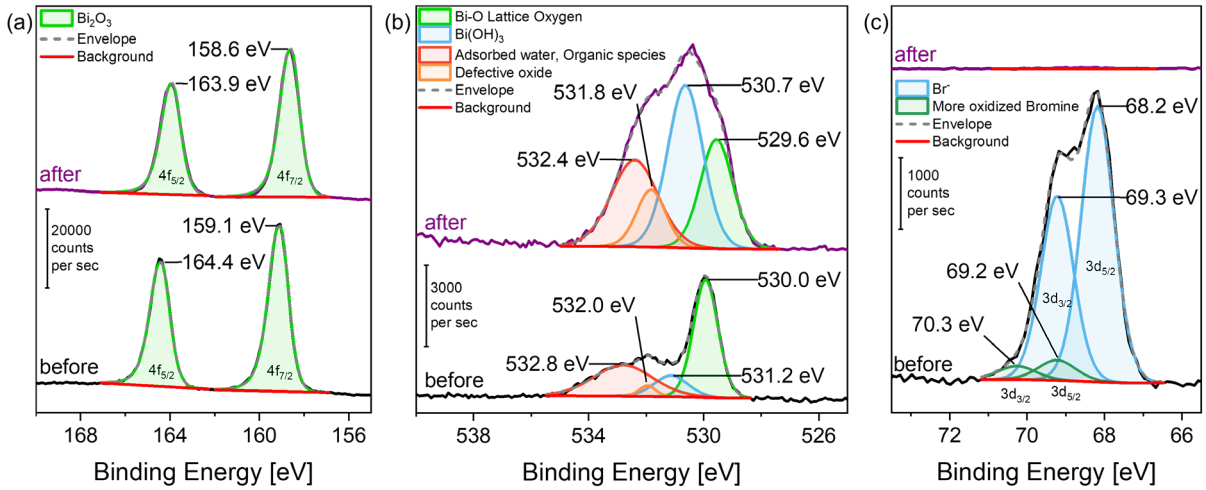

Figure S1. High-resolution XPS spectra of the Bi 4f (a), O 1s (b), and Br 3d (c) regions before and after electrolysis.

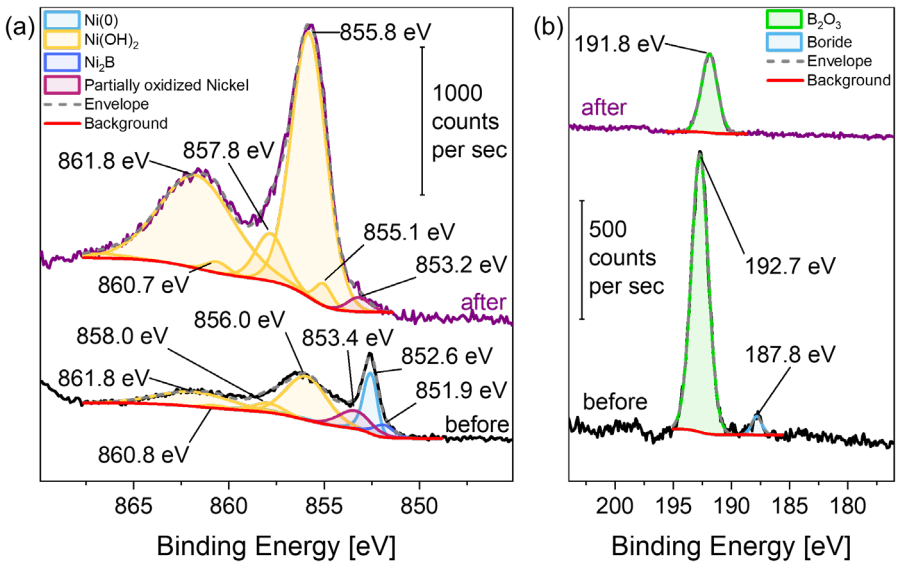

Figure S2. High-resolution XPS spectra of the Ni 2p (a) and B 1s (c) regions before and after electrolysis.

SEM results

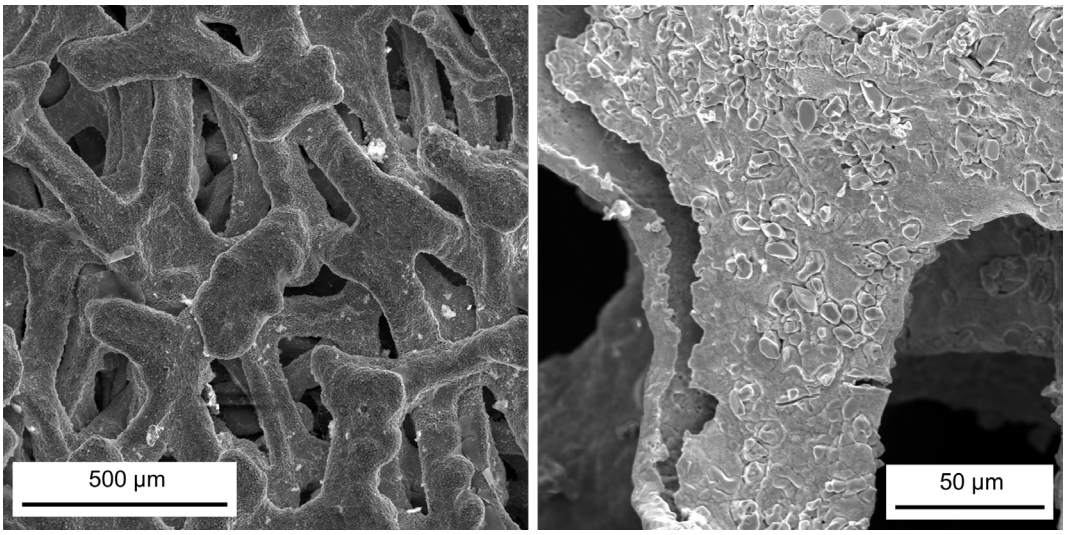

Figure S3. SEM micrographs of the Ni_xB anode after electrolysis at different magnifications.

ICP-MS results

Table S1. ICP-MS results for the Ni_xB electrode before and after electrolysis.

element	Ni_xB before		Ni_xB after	
	ppb	µmol L^{-1}	ppb	µmol L^{-1}
^{60}Ni	805360	13722.3	843760	14376.6
^{11}B	50098	4634.4	10780	997.2
total	855458	18356.7	854540	15373.8
Ni content	94.1	74.8	98.7	93.5
B content	5.9	25.2	1.3	6.5
total	100.0	100.0	100.0	100.0

From the ICP-MS results the initial Ni_xB composition was estimated as Ni_3B. After electrolysis, a smaller B content was determined, indicating that B dissolves during the electrolysis.

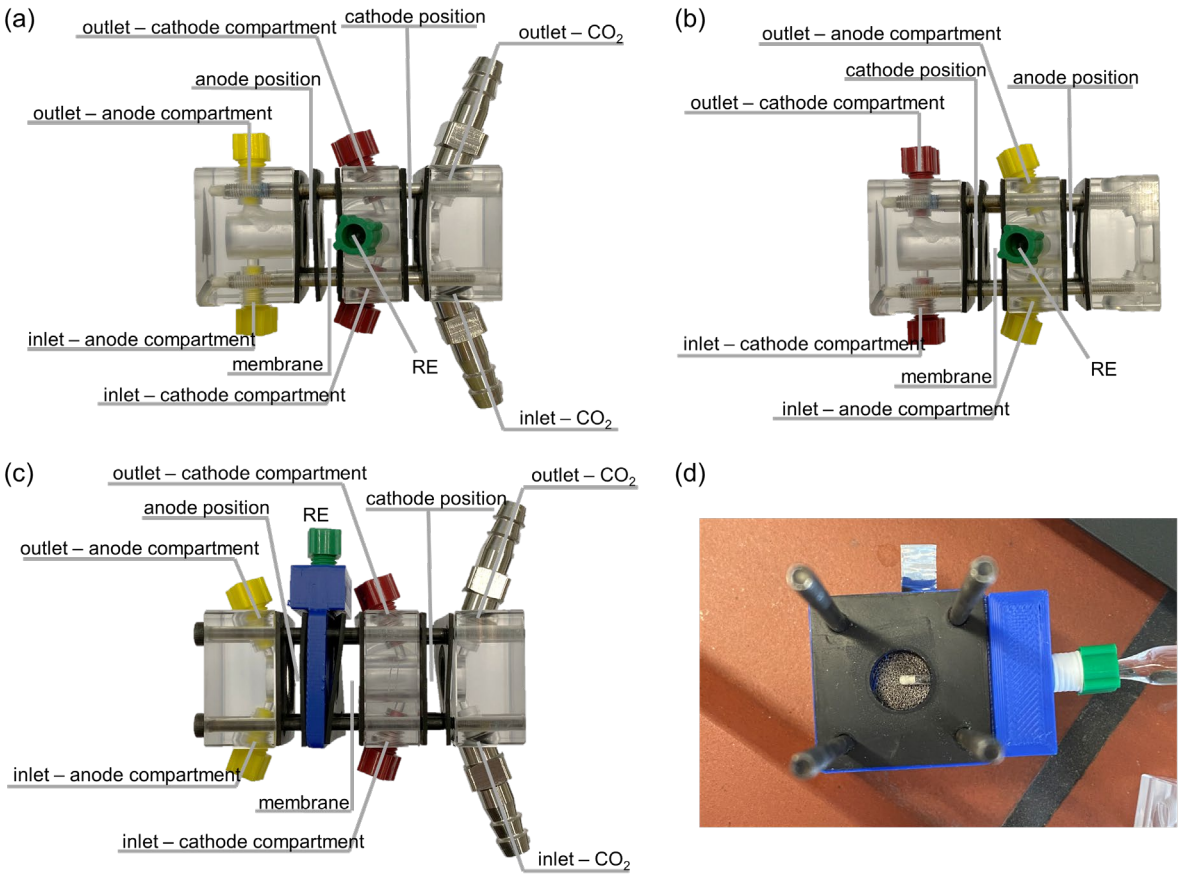

Figure S4. Images of the half-cell reactor for the OER||CO_2RR experiments (a), the GOR||HER experiments (b), and the paired electrolysis reactor for the GOR||CO_2RR experiments (c), and RE and Ni_xB anode (d).

Half-cell electrolysis

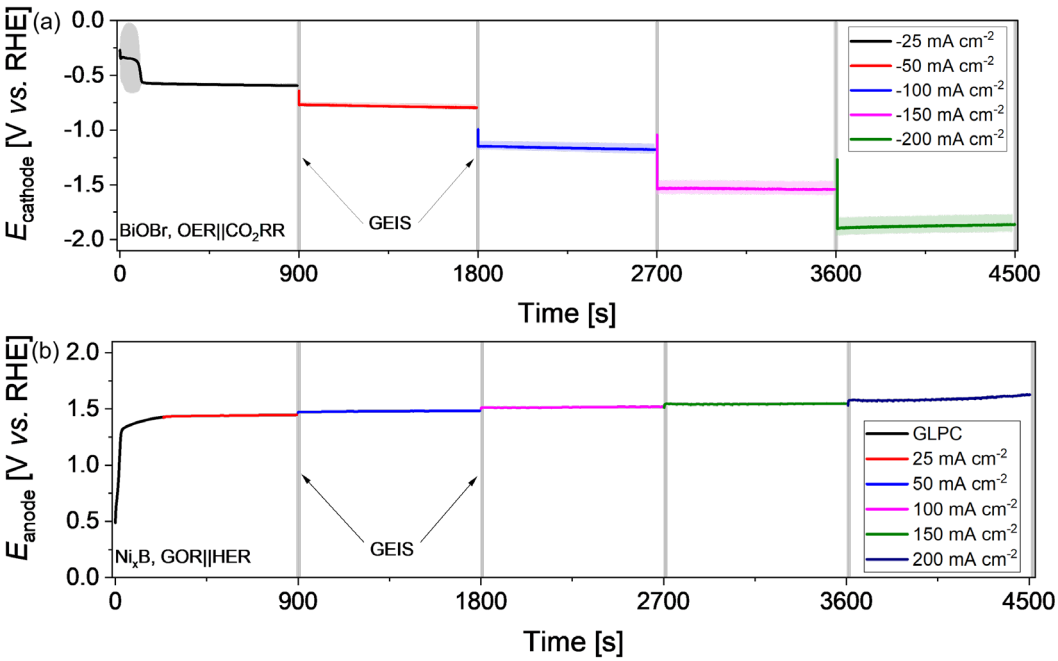

Figure S5. Average potentials recorded during half-cell electrolysis average $E_{cathode}$ BiOBr (a), and E_{anode} Ni_xB (b). Initially, a galvanostatic linear polarization curve (GLPC) from 0 to 25 mA cm^{-2} at 0.1 mA s^{-1} was recorded followed by chronopotentiometries at 25, 50, 100, 150 and 200 mA cm^{-2} for 14.88 min, and finally a galvanostatic electrochemical impedance spectroscopy from 100 kHz to 2 Hz with the amplitude current at 10 % of the applied current. Light grey lines are shown when GEIS was measured.

Table S2. Half-cell reactor average FE for H_2, CO, and HCO_2^-, and $E_{cathode}$ determined at different currents for BiOBr.

BiOBr	H_2		CO		HCO_2^-		$E_{cathode}$	
j [mA cm^{-2}]	FE [%]	st.dev.	FE [%]	st.dev.	FE [%]	st.dev.	V *vs.* RHE	st.dev.
-25	1.3	0.4	2.9	0.7	82.5	9.9	-0.6	0.0
-50	1.0	0.2	3.0	0.8	93.9	1.8	-0.8	0.0
-100	0.8	0.1	3.0	0.8	92.0	3.9	-1.2	0.0
-150	0.9	0.1	3.0	0.8	95.4	1.5	-1.5	0.1
-200	1.0	0.1	3.0	0.8	95.7	0.8	-1.9	0.1

Table S3. Half-cell reactor average FE for oxalate ($C_2O_4^{2-}$), tartronate ($C_3H_2O_5^{2-}$), glycerate ($C_3H_5O_4^-$), glycolate ($C_2H_3O_3^-$), lactate ($C_2H_5O_3^-$), formate (HCO_2^-), and acetate ($C_2H_3O_2^-$), and E_{anode} determined at different currents for Ni_xB.

Ni_xB	$C_2O_4^{2-}$	$C_3H_2O_5^{2-}$	$C_3H_5O_4^-$	$C_2H_3O_3^-$	$C_2H_5O_3^-$	HCO_2^-	$C_2H_3O_2^-$	E_{anode}
j [mA cm^{-2}]	FE [%]	FE [%]	FE [%]	FE [%]	FE [%]	FE [%]	FE [%]	V *vs.* RHE
25	0.5	0.0	12.3	14.6	3.6	71.2	0.1	1.5
50	1.6	0.0	11.0	11.9	4.6	67.3	0.6	1.5
100	4.2	0.0	8.7	13.2	3.4	54.4	0.5	1.5
150	6.3	0.1	8.2	13.5	2.1	50.8	0.5	1.6
200	6.6	0.1	8.9	12.2	0.3	48.3	0.0	1.6

Paired electrolysis

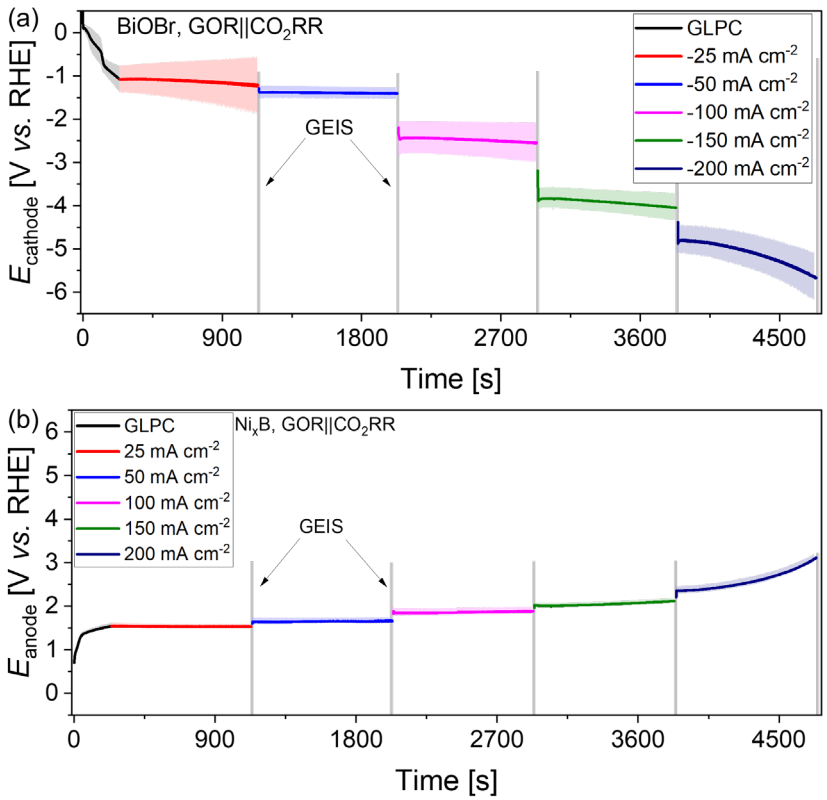

Figure S6. Average potentials recorded during paired electrolysis average $E_{cathode}$ BiOBr (a), and E_{anode} NixB (b). Average and standard deviations from 3 independent experiments. Initially, a galvanostatic linear polarization curve (GLPC) from 0 to 25 mA cm^{-2} at 0.1 mA s^{-1} was recorded followed by chronopotentiometries at 25, 50, 100, 150 and 200 mA cm^{-2} for 14.88 min, and finally a galvanostatic electrochemical impedance spectroscopy from 100 kHz to 2 Hz with the amplitude current at 10 % of the applied current. Light grey lines are shown when GEIS was measured.

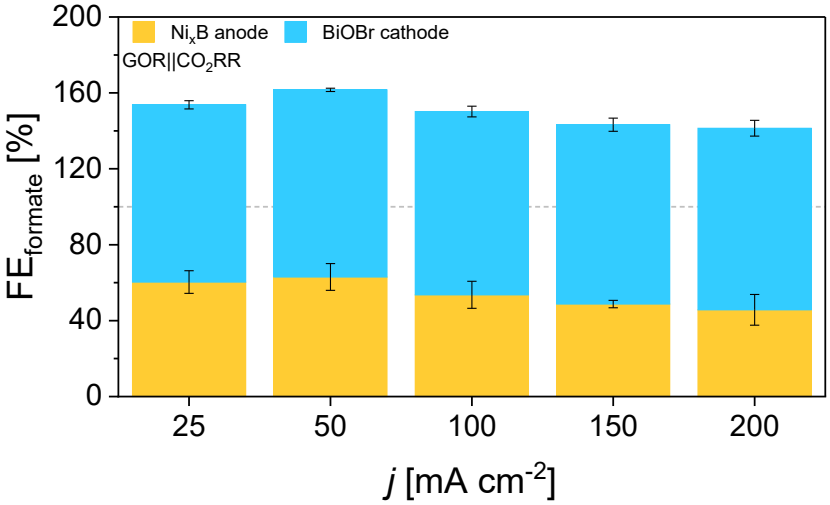

Figure S7. Average formate FE from paired electrolysis for the Ni_xB anode and BiOBr cathode. Average and standard deviations from 3 independent experiments. Values from Tables S4 and S5.

Table S4. Paired electrolyzer average FE for H_2, CO, and HCO_2^-, and $E_{cathode}$ determined at different currents for BiOBr. Average and standard deviations from 3 independent experiments.

BiOBr	H_2		CO		HCO_2^-		$E_{cathode}$	
j [mA cm^{-2}]	FE [%]	st.dev.	FE [%]	st.dev.	FE [%]	st.dev.	V *vs.* RHE	st.dev.
-25	0.6	0.2	3.2	0.3	93.4	2.2	-1.2	0.6
-50	0.6	0.2	3.4	0.3	98.6	0.9	-1.4	0.1
-100	0.7	0.2	3.5	0.2	96.6	2.8	-2.6	0.4
-150	0.8	0.5	3.4	0.3	94.5	3.5	-4.1	0.3
-200	1.0	0.5	3.5	0.3	95.7	4.2	-5.7	0.5

Table S5. Paired electrolyzer average FE for oxalate ($C_2O_4^{2-}$), tartronate ($C_3H_2O_5^{2-}$), glycerate ($C_3H_5O_4^-$), glycolate ($C_2H_3O_3^-$), lactate ($C_2H_5O_3^-$), formate (HCO_2^-), and acetate ($C_2H_3O_2^-$), and E_{anode} determined at different currents for Ni_xB. Average and standard deviations from 3 independent experiments.

Ni_xB	$C_2O_4^{2-}$		$C_3H_2O_5^{2-}$		$C_3H_5O_4^-$		$C_2H_3O_3^-$		$C_2H_5O_3^-$		HCO_2^-		$C_2H_3O_2^-$		E_{anode}	
j [mA cm^{-2}]	FE [%]	st.dev.	FE [%]	st.dev.	FE [%]	st.dev.	FE [%]	st.dev.	FE [%]	st.dev.	FE [%]	st.dev.	FE [%]	st.dev.	V *vs.* RHE	st.dev.
25	0.5	0.2	0.0	0.0	6.3	1.3	21.2	1.9	1.2	0.8	60.3	6.0	0.0	0.4	1.5	0.0
50	2.2	1.9	0.0	0.0	9.0	2.9	13.6	2.5	4.8	2.1	63.0	7.0	0.1	0.2	1.7	0.1
100	4.6	1.3	0.0	0.0	7.7	1.8	12.5	3.2	4.6	1.3	53.6	7.1	0.1	0.2	1.9	0.1
150	6.8	0.3	0.1	0.0	7.6	0.9	11.7	1.2	1.2	0.2	48.8	1.9	0.2	0.1	2.1	0.0
200	7.0	1.4	0.1	0.0	6.3	0.6	13.2	2.5	0.2	0.6	45.7	8.1	0.1	0.0	3.1	0.1

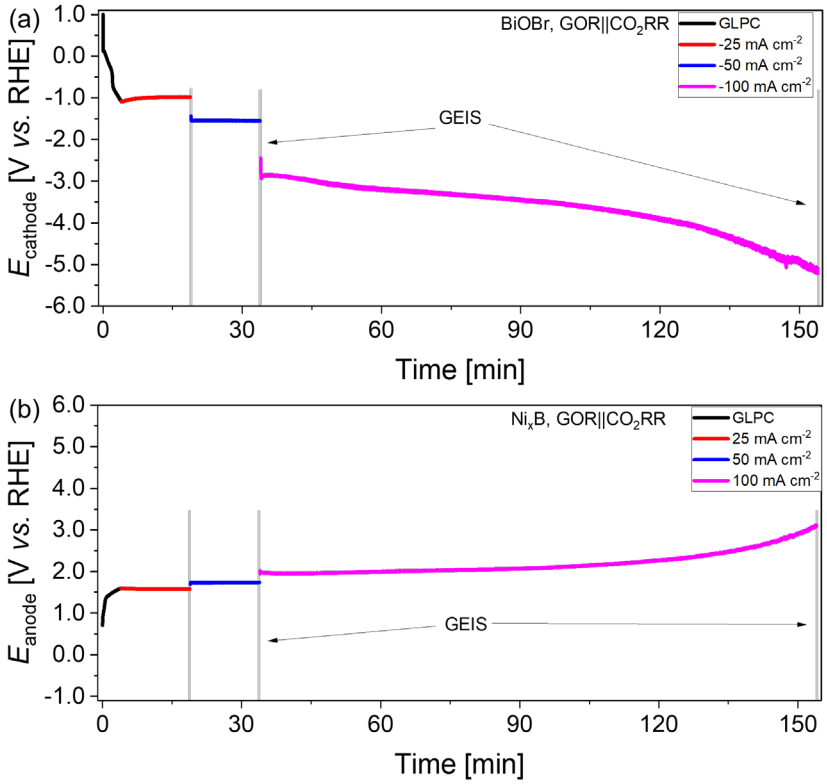

Figure S8. Average potential recorded in paired electrolyzer average $E_{cathode}$ BiOBr (a), and E_{anode} Ni_xB (b) determined at different currents for 2.5 h. Initially, a galvanostatic linear polarization curve (GLPC) from 0 to 25 mA cm^{-2} at 0.1 mA s^{-1} was recorded followed by chronopotentiometries at 25, 50, and 100 mA cm^{-2} for different times, and finally a galvanostatic electrochemical impedance spectroscopy from 100 kHz to 2 Hz with the amplitude current at 10 % of the applied current. Light grey lines are shown when GEIS was measured.

Table S6. Paired electrolyzer FE for H_2, CO, and HCO_2^-, and $E_{cathode}$ determined at different currents for 2.5 h for BiOBr.

BiOBr		H_2	CO	HCO_2^-	$E_{cathode}$
Time [min]	j [mA cm^{-2}]	FE [%]	FE [%]	FE [%]	V *vs.* RHE
15	-25	0.5	3.5	93.4	-1.0
30	-50	0.4	3.7	97.8	-1.6
45	-100	0.6	3.7	94.5	-3.1
60	-100	0.8	3.7	97.4	-3.2
90	-100	1.3	3.7	98.2	-3.5
120	-100	1.5	3.8	100.1	-4.0
150	-100	1.7	3.8	91.5	-5.1

Table S7. Paired electrolyzer FE for oxalate ($C_2O_4^{2-}$), tartronate ($C_3H_2O_5^{2-}$), glycerate ($C_3H_5O_4^-$), glycolate ($C_2H_3O_3^-$), lactate ($C_2H_5O_3^-$), formate (HCO_2^-), and acetate ($C_2H_3O_2^-$), and E_{anode} determined at different currents for 2.5 h for Ni_xB.

Ni_xB		$C_2O_4^{2-}$	$C_3H_2O_5^{2-}$	$C_3H_5O_4^-$	$C_2H_3O_3^-$	$C_2H_5O_3^-$	HCO_2^-	$C_2H_3O_2^-$	E_{anode}
Time [min]	j [mA cm^{-2}]	FE [%]	FE [%]	FE [%]	FE [%]	FE [%]	FE [%]	FE [%]	V *vs.* RHE
15	25	0.4	0.0	5.7	18.4	0.3	66.4	0.0	1.6
30	50	1.8	0.0	9.3	13.7	7.0	68.9	0.0	1.7
45	100	6.1	0.0	9.7	16.2	5.8	59.8	0.3	2.0
60	100	6.4	0.0	7.9	12.6	3.9	50.6	0.2	2.0
90	1000	7.4	0.1	7.1	13.6	3.1	57.9	0.0	2.1
120	100	6.1	0.1	6.2	12.4	0.5	59.9	0.2	2.3
150	100	4.2	0.1	6.3	12.8	0.7	55.0	0.0	3.1

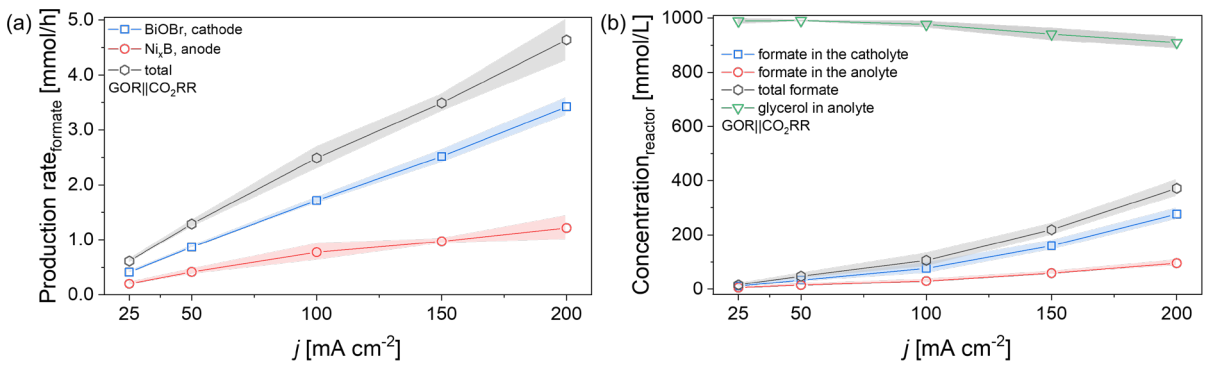

Figure S9. Paired electrolyzer formate production rate (a), and formate and glycerol concentration in the reactor (b) for BiOBr cathode and Ni_xB anode. Average and standard deviations from 3 independent experiments.

Comparison

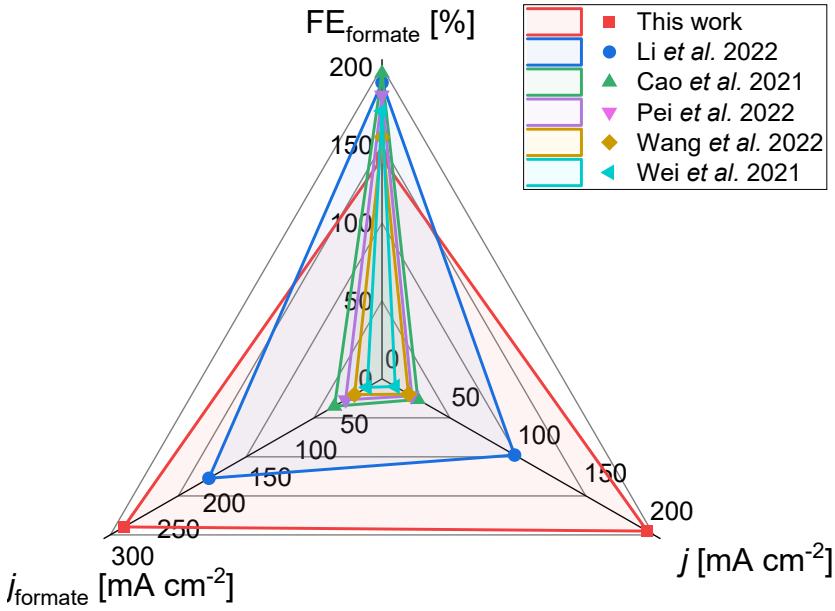

Figure S10. Comparison of total FE in paired electrolysers for formate (anode + cathode), measured current density, and total formate partial current density (anode + cathode) between this work and other recent publications: Li *et al.* 2022,[1] Cao *et al.* 2021,[2] Pei *et al.* 2022,[3] Wang *et al.* 2022,[4] and Wei *et al.* 2021 (a).[5] Values summarized in Table S8.

Table S8. Comparison of values for the total formate selectivity, paired electrolyzer operation current density and total formate partial current density between this work and other recent publications about paired electrolyzer for formate production: Li *et al.* 2022,[1] Cao *et al.* 2021,[2] Pei *et al.* 2022,[3] Wang *et al.* 2022,[4] and Wei *et al.* 2021.[5] Anode reactions: glycerol oxidation reaction (GOR), formaldehyde oxidation reaction (FOR), methanol oxidation reaction (MOR), and PET oxidation reaction (POR).

	Anode reaction	total formate selectivity [%]	j_{geo} [mA cm^{-2}]	$j_{formate}$ [mA cm^{-2}]
This work	GOR	141.4	200.0	282.8
Li *et al.* 2022[1]	FOR	190.0	100.0	190.0
Cao *et al.* 2021[2]	MOR	196.0	27.0	52.9
Pei *et al.* 2022[3]	GOR	182.0	22.4	40.8
Wang *et al.* 2022[4]	POR	155.0	20.0	31.0
Wei *et al.* 2021[5]	MOR	171.8	10.0	17.2

CO_2 reduction half-cell reactions

carbon monoxide	$CO_2 + 2H_2O + 2e^- \longrightarrow CO + 2OH^-$	(S1)
formate	$CO_2 + H_2O + 2e^- \longrightarrow HCO_2^- + OH^-$	(S2)
hydrogen evolution	$2H_2O + 2e^- \longrightarrow H_2 + 2OH^-$	(S3)

Glycerol oxidation half-cell reactions [6]

acetate	$C_3H_8O_3 + 7/2\ OH^- \rightarrow 3/2\ C_2H_3O_2^- + 7/2\ H_2O + 2\ e^-$	(S4)
lactate	$C_3H_8O_3 + 7/2\ OH^- \rightarrow 3/2\ C_2H_5O_3^- + 2\ H_2O + 2\ e^-$	(S5)
glycerate	$C_3H_8O_3 + 5\ OH^- \rightarrow 1\ C_3H_5O_4^- + 4\ H_2O + 4\ e^-$	(S6)
glycolate	$C_3H_8O_3 + 13/2\ OH^- \rightarrow 3/2\ C_2H_3O_3^- + 5\ H_2O + 5\ e^-$	(S7)
formate	$C_3H_8O_3 + 11\ OH^- \rightarrow 3\ HCO_2^- + 8\ H_2O + 8\ e^-$	(S8)
tartronate	$C_3H_8O_3 + 10\ OH^- \rightarrow 1\ C_3H_2O_5^{2-} + 8\ H_2O + 8\ e^-$	(S9)
oxalate	$C_3H_8O_3 + 14\ OH^- \rightarrow 3/2\ C_2O_4^{2-} + 11\ H_2O + 11\ e^-$	(S10)
carbon dioxide	$C_3H_8O_3 + 14\ OH^- \rightarrow 3\ CO_2 + 11\ H_2O + 14\ e^-$	(S11)

Energy-efficiency calculation

To determine the energy-efficiency of the measured systems was calculated using equation S12:

$$\text{Energy-efficiency} = \frac{n_{\text{formate}} \times \Delta H^0_{\text{formate}}}{E_{\text{cell}} \times Q} \tag{S12}$$

n_{formate} is the total produced mols of formate (anode + cathode) in mol, $\Delta H^0_{\text{formate}}$ the formate heat of combustion (278.2 kJ mol^{-1}) in J mol^{-1}, E_{cell} the cell voltage ($E_{\text{cell}} = E_{\text{anode}} - E_{\text{cathode}}$) in V, and Q the charge (Q = i * t) in C. The formate heat of combustion, $\Delta H^0_{\text{formate}}$ was determined using equation S13:

$$\Delta H^0_{\text{formate}}(298.15\ \text{K}) = \left|\Delta_f H^0(CO_2) + \frac{1}{2}\Delta_f H^0(H_2O) - \Delta_f H^0(HCO_2^-) - \frac{1}{4}\Delta_f H^0(O_2)\right| \tag{S13}$$

formate combustion $\quad 4HCO_2^- + 1O_2(g) \rightarrow 4CO_2(g) + 2H_2O(l)$ (S14)

Where $\Delta_f H^0\ (CO_2)$ = -393.476 kJ mol^{-1}, $\Delta_f H^0\ (H_2O)$ = -285.796 kJ mol^{-1}, $\Delta_f H^0\ (HCO_2^-)$ = -466.8 kJ mol^{-1}, and $\Delta_f H^0\ (O_2)$ = 0.0 kJ mol^{-1}. Values from the Active Thermochemical Tables version 1.124.[7]

Table S9. Results of the energy-efficiency calculations for the paired electrolyte performing GOR||CO_2RR (a), half-cell performing OER||CO_2RR (b), and GOR||HER (c). The relative energy-efficiency of the different reactors configurations (d) at different applied current densities.

(a)	GOR||CO_2RR							
j [mA cm^{-2}]	n_{formate} [mol]			E_{cell} [V]	Q [C]	formate energy [J]	input energy [J]	Energy-efficiency
	cathode	anode	total					
25	1.03E-04	5.01E-05	1.53E-04	2.66	21.2	10.7	56.4	18.9
50	2.17E-04	1.05E-04	3.22E-04	3.04	42.4	22.4	128.9	17.4
100	4.29E-04	1.78E-04	6.07E-04	4.33	84.8	42.2	367.6	11.5
150	6.30E-04	2.43E-04	8.73E-04	5.95	127.1	60.7	756.4	8.0
200	8.56E-04	3.04E-04	1.16E-03	7.67	169.5	80.7	1299.3	6.2

(b)	OER||CO_2RR							
j [mA cm^{-2}]	n_{formate} [mol]			E_{cell} [V]	Q [C]	formate energy [J]	input energy [J]	Energy-efficiency
	cathode	anode	total					
25	9.12E-05	-	9.12E-05	1.50	21.2	6.3	31.8	20.0
50	2.08E-04	-	2.08E-04	3.06	42.4	14.5	129.6	11.2
100	4.08E-04	-	4.08E-04	4.45	84.8	28.4	377.6	7.5
150	6.31E-04	-	6.31E-04	6.15	127.1	43.9	782.2	5.6
200	8.46E-04	-	8.46E-04	7.89	169.5	58.8	1336.7	4.4

(c)	GOR||HER							
j [mA cm^{-2}]	$n_{formate}$ [mol]			E_{cell} [V]	Q [C]	formate energy [J]	input energy [J]	Energy-efficiency
	cathode	anode	total					
25	-	5.91E-05	5.91E-05	3.09	21.2	4.1	65.5	6.3
50	-	1.12E-04	1.12E-04	3.52	42.4	7.8	149.0	5.2
100	-	1.81E-04	1.81E-04	4.19	84.8	12.6	355.7	3.5
150	-	2.53E-04	2.53E-04	4.99	127.1	17.6	634.8	2.8
200	-	3.21E-04	3.21E-04	6.42	169.5	22.3	1088.8	2.1

(d)	Relative energy-efficiency [%]	
j [mA cm^{-2}]	GOR||CO_2RR *vs.* OER||CO_2RR	GOR||CO_2RR *vs.* GOR||HER
25	-5.2	201.7
50	55.5	233.0
100	52.8	225.0
150	43.0	189.0
200	41.0	202.8

These calculations show that the used paired electrolyze performing GOR||CO_2RR is in general more energy-efficient when compared to the OER||CO_2RR and GOR||HER reactors. Considering the total formate production of each kind of reactor, at 200 mA cm^{-2}, the paired electrolyzer is 41 % more energy efficient that the OER||CO_2RR, and 203 % more energy efficient than the GOR||HER reactor.

CO_2 balance estimation

The CO_2 balance estimation was calculated with equation S15.

$$\mathrm{CO_2\ balance} = \mathrm{mol_{CO_2}\,produced\ from\ glycerol\ oxidation} - \mathrm{mol_{CO_2}\,consumed\ from\ formate\ production} \quad \text{(S15)}$$

During the experiments on the GOR side, two possible products were not analyzed. The first one is O_2 from the competitive OER and the second one is CO_2 from the complete glycerol oxidation. Since these products were not analyzed, it is only possible to determine their production. From the HPLC results there is a substantial missing FE on the anode side, which is assumed to come from the presence of the non-analyzed gaseous products O_2 and CO_2. For the CO_2 balance estimation, it was considered that the Ni_xB on Ni foam electrode does not perform any OER, so all the missing FE results from the complete glycerol oxidation. Therefore, at 200 mA cm^{-2} the FE for CO_2 at the anode is around 33.9 %. From equation S11, there are 14 electrons involved in the complete oxidation of glycerol to CO_2 and the stoichiometric factor is 3, this results in a maximal production of CO_2 of 1.28 x10^{-4} mol (over a 15-minute-long experiment, resulting in 5.12 x10^{-4} mol h^{-1}) or 1.25 x10^{-5} m^3 h^{-1} (12.5 mL h^{-1}).

On the CO_2RR side, gaseous CO_2 is fixed into liquid formate. From the HPLC results at 200 mA cm^{-2}, there is an average formate production of 8.56 x10^{-4} mol (over 15 minutes long experiment, resulting in 3.42 x10^{-3} mol h^{-1}). This results in a CO_2 consumption of around 8.37 x10^{-5} m^3 h^{-1} (83.7 mL h^{-1}) at the cathode.

The presented paired electrolyzer at 200 mA cm^{-2} shows a CO_2 balance of -7.28 x10^{-4} mol (over a 15-minute-long experiment, resulting in -2.91 x10^{-3} mol h^{-1}) or -7.12 x10^{-5} m^3 h^{-1} (-71.2 mL h^{-1}). This estimation demonstrates that the paired electrolyze consumes more CO_2 than it releases in the order of 2.91 x10^{-3} mol h^{-1}. The values were calculated using the ideal gas law and considering 25 °C and 1 atm as ambient temperature and pressure.

Table S10. The estimated CO_2 production at the anode from the glycerol complete oxidation (a), the measured CO_2 consumption at the from the formate production (b), and the estimation of the CO_2 balance (c) at different current densities and with different units.

(a)	CO_2 produced from glycerol complete oxidation			
j [mA cm^{-2}]	mol in 15 min	mol h^{-1}	m^3 h^{-1}	mL h^{-1}
25	5.39E-06	2.16E-05	5.28E-07	0.5
50	9.18E-06	3.67E-05	8.99E-07	0.9
100	2.68E-05	1.07E-04	2.62E-06	2.6
150	7.96E-05	3.19E-04	7.79E-06	7.8
200	1.28E-04	5.11E-04	1.25E-05	12.5

(b)	CO_2 consumed from formate production			
j [mA cm^{-2}]	mol in 15 min	mol h^{-1}	m^3 h^{-1}	mL h^{-1}
25	1.03E-04	4.13E-04	1.01E-05	10.1
50	2.17E-04	8.69E-04	2.13E-05	21.3
100	4.29E-04	1.72E-03	4.20E-05	42.0
150	6.30E-04	2.52E-03	6.16E-05	61.6
200	8.56E-04	3.42E-03	8.37E-05	83.7

(c)	CO_2 balance			
j [mA cm^{-2}]	mol in 15 min	mol h^{-1}	m^3 h^{-1}	mL h^{-1}
25	-9.79E-05	-3.92E-04	-9.58E-06	-9.58
50	-2.08E-04	-8.32E-04	-2.04E-05	-20.37
100	-4.02E-04	-1.61E-03	-3.93E-05	-39.34
150	-5.50E-04	-2.20E-03	-5.38E-05	-53.83
200	-7.28E-04	-2.91E-03	-7.12E-05	-71.24

References

[1] M. Li, T. Wang, W. Zhao, S. Wang, Y. Zou, *Nano-Micro Lett.* **2022**, *14*, 211.
[2] C. Cao, D.-D. Ma, J. Jia, Q. Xu, X.-T. Wu, Q.-L. Zhu, *Adv. Mater.* **2021**, *33*, e2008631.
[3] Y. Pei, Z. Pi, H. Zhong, J. Cheng, F. Jin, *J. Mater. Chem. A* **2022**, *10*, 1309.
[4] J. Wang, X. Li, M. Wang, T. Zhang, X. Chai, J. Lu, T. Wang, Y. Zhao, D. Ma, *ACS Catal.* **2022**, *12*, 6722.
[5] X. Wei, Y. Li, L. Chen, J. Shi, *Angew. Chem. Int. Ed.* **2021**, *60*, 3148.
[6] X. Han, H. Sheng, C. Yu, T. W. Walker, G. W. Huber, J. Qiu, S. Jin, *ACS Catal.* **2020**, *10*, 6741.
[7] "Active Thermochemical Tables (ATcT) version 1.124", can be found under https://atct.anl.gov/Thermochemical%20Data/version%201.124/index.php.